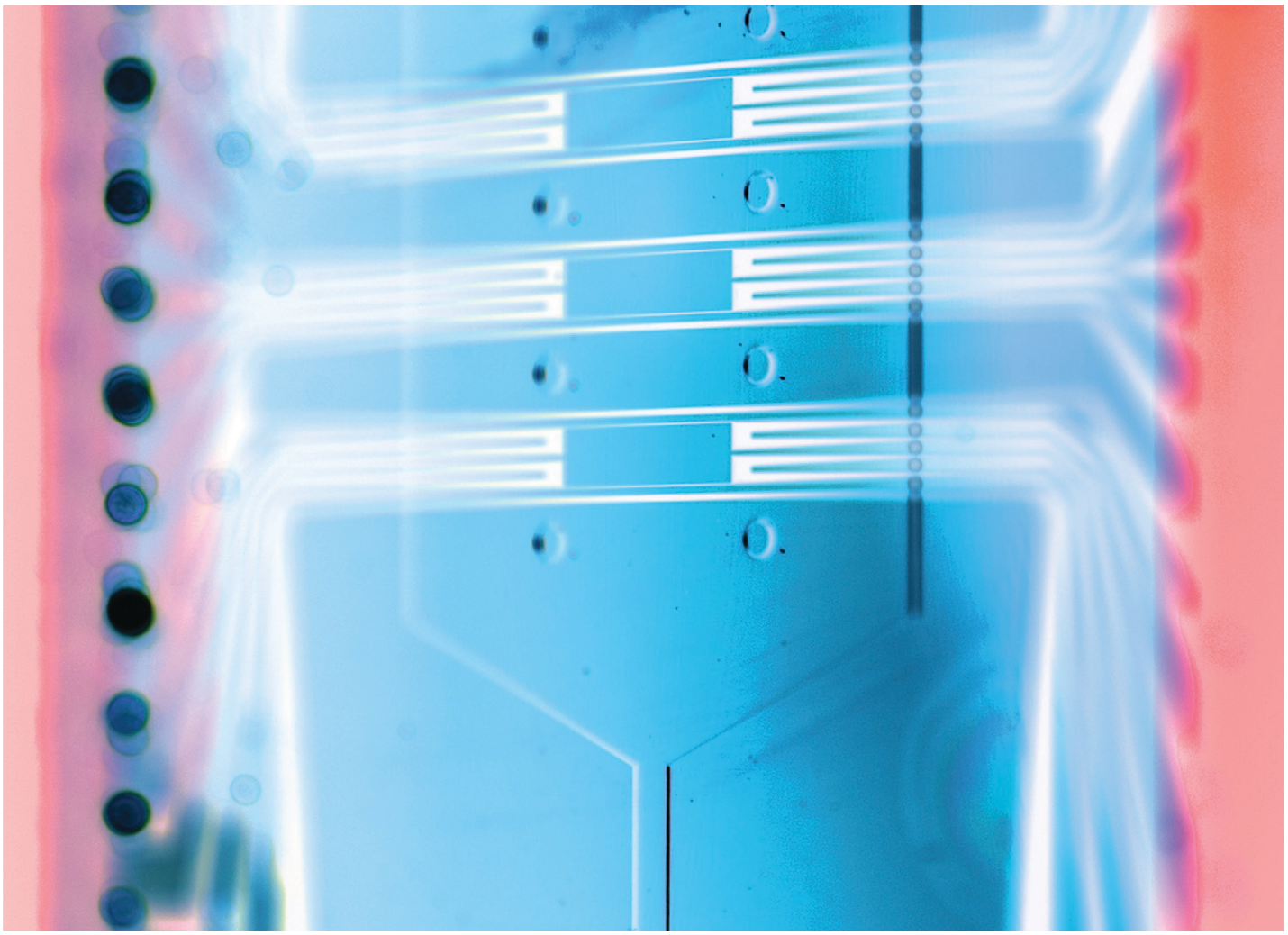

Featuring work from the Tenje and Behrendt labs at Uppsala University.

A microscopy-compatible temperature regulation system for single-cell phenotype analysis – demonstrated by thermoresponse mapping of microalgae

A temperature control stage for single-cell microscopy mapping thermoresponse of algea.

As featured in:

See Lars Behrendt, Maria Tenje *et al.*, *Lab Chip*, 2021, **21**, 1694.

ROYAL SOCIETY OF CHEMISTRY

rsc.li/loc

Registered charity number: 207890

Lab on a Chip

PAPER

View Article Online
View Journal | View Issue

Cite this: *Lab Chip*, 2021, **21**, 1694

A microscopy-compatible temperature regulation system for single-cell phenotype analysis – demonstrated by thermoresponse mapping of microalgae†

Martin Andersson, ‡[a] Sofia Johansson, ‡[a] Henrik Bergman, [a] Linhong Xiao, [b] Lars Behrendt *[b] and Maria Tenje *[a]

This work describes a programmable heat-stage compatible with *in situ* microscopy for the accurate provision of spatiotemporally defined temperatures to different microfluidic devices. The heat-stage comprises an array of integrated thin-film Joule heaters and resistance temperature detectors (RTDs). External programming of the heat-stage is provided by a custom software program connected to temperature controllers and heater–sensor pairs. Biologically relevant (20–40 °C) temperature profiles can be supplied to cells within microfluidic devices as spatial gradients (0.5–1.5 °C mm^{-1}) or in a time-varying approach *via e.g.* step-wise or sinusoidally varying profiles with negligible temperature over-shoot. Demonstration of the device is achieved by exposing two strains of the coral symbiont *Symbiodinium* to different temperature profiles while monitoring their single-cell photophysiology *via* chlorophyll fluorometry. This revealed that photophysiological responses to temperature depended on the exposure duration, exposure magnitude and strain background. Moreover, thermal dose analysis suggested that cell acclimatisation occurs under longer temperature (6 h) exposures but not under shorter temperature exposures (15 min). As the thermal sensitivity of *Symbiodinium* mediates the thermal tolerance in corals, our versatile technology now provides unique possibilities to research this interdependency at single cell resolution. Our results also show the potential of this heat-stage for further applications in fields such as biotechnology and ecotoxicology.

Received 18th December 2020,
Accepted 22nd March 2021

DOI: 10.1039/d0lc01288b

rsc.li/loc

Introduction

Temperature influences the physiology of living organisms and sets the binding constraints for biochemical reactions, metabolism, growth, development and reproduction.[1] Where endothermic organisms have developed advanced internal temperature regulation systems to account for environmental temperature variations, ectotherms (*e.g.* microorganisms) lack this regulation and are thus predicted to be more severely affected by rising temperatures provoked by climate change.

The increasing frequency of warming events causes biological impacts across our planet and one ecosystem particularly afflicted by thermal stress is coral reefs, one of the most biodiverse and productive ecosystems. Corals gain >70% of their energy through a symbiotic relationship with photosynthetic microalgae from the genus *Symbiodiniaceae* (*Dinoflagellata*).[2] Increasing temperatures can provoke coral 'bleaching', a process by which *Symbiodinium* disappears from the coral tissue through an essentially unknown mechanism. The frequency of these bleaching events has increased over the past decades and coral reefs are now facing near extinction due to the effects of global warming. The severity of bleaching is intimately linked to the thermal resilience of *Symbiodinium*, which has been intensively studied on the bulk level within and between species.[3,4] Proposed strategies for mitigating coral bleaching include rearing coral stocks with enhanced stress tolerance *via* assisted evolution[5,6] or experimental evolution of *Symbiodinium* cultivars.[7] These strategies, however, seldom take into account the phenotypic heterogeneity among single cells of *Symbiodinium*, which could reveal genotypes with increased resistance towards environmental stress as found in, *e.g.*, bacterial populations.[8] Mapping the photosynthetic response of single-cells of *Symbiodinium* under thermal stress

[a] *Dept. Materials Science and Engineering, Science for Life Laboratory, Uppsala University, Box 35, 751 03 Uppsala, Sweden. E-mail: maria.tenje@angstrom.uu.se*
[b] *Dept. Organismal Biology, Science for Life Laboratory, Uppsala University, Norbyvägen 18 A, 752 36 Uppsala, Sweden. E-mail: lars.behrendt@scilifelab.uu.se*
† Electronic supplementary information (ESI) available. See DOI: 10.1039/d0lc01288b
‡ M. Andersson and S. Johansson should be considered joint first author.

in vitro could therefore have immediate consequences for our understanding of coral thermal resilience *in situ* and could possibly provide new avenues for coral reef restoration.

Microfluidics has emerged as a key technology for characterizing phenotypic variations in populations of single cells under external perturbations. For example, microfluidic platforms are used to measure viability and Ca^{2+} flux of single mammalian cells,[9] map real-time growth rates of single bacteria to monitor antibiotic susceptibility[10] and determine phenotypes of single microalgal cells co-cultured with bacteria.[11] Key to this success is the ability of microfluidic platforms to physically immobilize several thousands of single cells, often using hydrodynamic forces or mechanical features such as wells, pillars or channel restrictions at precisely defined locations[12] and then deliver external physico-chemical stimuli to those same sites. Stimuli can be in the form of drugs or toxins delivered *via* integrated microfluidic channels or pressure delivered *via* integrated microelectromechanical actuators.[13] Due to the small size of microfluidic channels, only minimal sample and reagent volumes are required, which reduces costs, shortens reaction times and enables biochemical studies where sample materials are scarce.

To reliably measure the effects of thermal stress on organisms within microfluidic systems, providing accurate temperatures is essential. One approach is to mount the microfluidic system inside a small incubator providing a well-defined and stable temperature.[14–17] However, these systems often require long ramping times and offer limited possibilities to cycle temperatures or deliver well-defined gradients of temperatures across the microfluidic devices. For precise temperature control on-chip, miniaturised heaters are typically used, such as Joule heaters increasing the temperature through conversion of electrical energy to heat *via* resistive losses.[18] Several microfluidic systems use this principle of operation *via* microstructured thin-film metal electrodes,[19,20] screen printed electrodes[21] or conductive liquids.[22] However, these systems integrate the temperature control within the microfluidic device and are typically developed for a single application, meaning that their use in other areas is limited. Further, sterility requirements often limit them to single-use, which increases costs and reduces usability of these temperature control systems.

Here, we present a reusable modular temperature regulation system that can be combined with interchangeable microfluidic systems of various designs. By placing the microfluidic chip immediately on the temperature control stage *via* a thin film of immersion oil and using active liquid cooling, a powerful and versatile system with spatiotemporal temperature regulation is created. This represents a technological advancement over more rigid fixed-design systems where the temperature control and microfluidics device are combined. The facile chip mounting is achieved by providing a flat surface by using thin-film Joule heaters and RTDs, recessed into the top glass plate of the heat-stage. The temperature regulation system is capable of providing stable temperatures in the range of 20–40 °C to cells immobilized within microfluidic chips. Importantly, biologically relevant temperatures can be supplied to the cells in the form of spatial gradients or in a dynamic, time-varying fashion. In this study, the functionality of the temperature regulation system was demonstrated by combining it with a microfluidic device with an array of 16 500 individual microwells containing single cells of two strains of *Symbiodinium*. The photophysiological changes occurring in single cells under temperature perturbations were assessed *via* pulse amplitude modulated chlorophyll fluorometry (PAM) imaging. We suggest that this novel engineering approach provides a powerful and versatile platform for single cell investigations of photosynthetic stress resilience and heterogeneity under recreated spatiotemporal thermal exposure profiles.

Results and discussion

Temperature regulation system

A programmable temperature regulation system was developed to provide spatiotemporal temperature control in interchangeable microfluidic devices. The temperature regulation system comprises four main parts: i) a heat-stage with an integrated array of Joule heaters and resistance temperature detectors (RTDs), ii) a temperature controller, which regulates the applied power given to the individual heaters, iii) a GUI software program, which allows the user to apply desired temperature profiles and gradients and iv) a liquid cooling system, which improves the temperature ramping times and thermal stability through increased heat dissipation (Fig. 1). The system is compatible with transmission and fluorescence microscopy by providing a 6.0 mm by 8.5 mm optically transparent window intersecting the temperature controlled area. The system can deliver a range of time-varying temperature profiles including step-wise increasing and sinusoidally cycled temperatures. It can also deliver spatial temperature gradients across microfluidic devices (Fig. 2). In the following, we first describe the design and functionality of the temperature regulation system and then report and discuss results from experiments in which *Symbiodinium* cells were exposed to thermal stress.

Design and fabrication. The temperature of the heat-stage is regulated through six individually controlled thin-film heaters and RTDs. The heaters and temperature sensors were integrated onto the glass heat-stage by evaporation and patterning of Ni into line electrodes using UV lithography (Fig. 1C). The electrodes were recessed into the glass substrate through wet etching prior to Ni evaporation, resulting in a flat surface.[23] Each Joule heater stretched well outside of the temperature control window with a length of 19 mm to provide a uniform temperature in the active area. The heater width was 12 μm and the heater–heater spacing 1.3 mm. The design matched that of the microfluidic chip containing three separated areas with single-cell arrays, so that each array was placed in between two heaters. RTDs

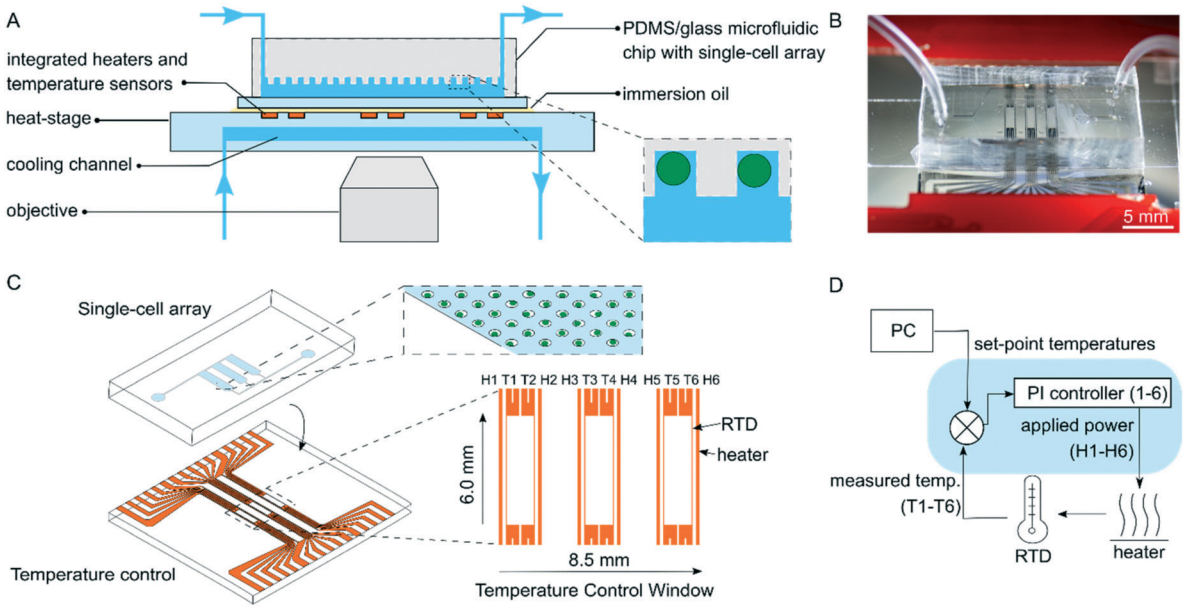

Fig. 1 A programmable temperature regulation system with an attached microfluidic chip. (A) Cross-section of the temperature regulation system placed under a microscope with a mounted microfluidic chip. The inset depicts immobilized single microalgae in microwell geometries within the microfluidic chip. (B) A photograph of the heat-stage with an attached PDMS/glass microfluidic chip. (C) Attachment of the microfluidic chip on the heat-stage. The upper inset displays a single cell array and the lower inset the design of the heater and temperature sensor arrays in the actively heated area, here referred to as the temperature control window. (D) Schematic of the different parts of the temperature regulation system. Using the temperature controller, the power applied to each heater is individually regulated *via* a feedback loop, which reads the temperature of the neighboring temperature sensor.

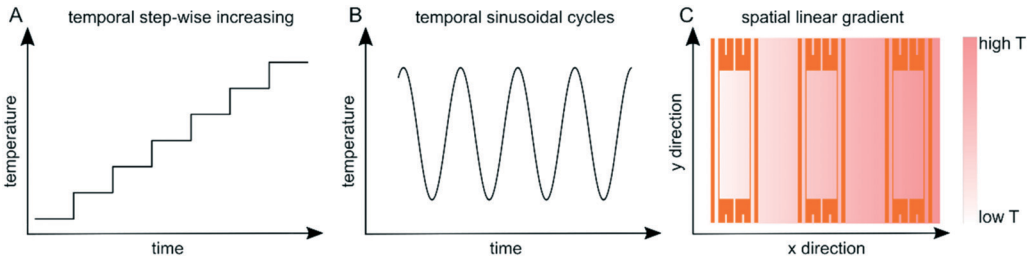

Fig. 2 Examples of thermal profiles generated with the temperature regulation system. (A) Step-wise increasing temperature over time. (B) Sinusoidally varying temperature over time, and (C) a linear gradient across the whole temperature regulated area.

were placed just inside of each heater with a width of 5 μm and with a heater–sensor spacing of 12 μm. The length of the RTD line electrodes was 4 mm and on each end the electrode width increased and split up to enable 4-point measurements (Fig. S5†). Joule heating was accomplished by applying voltages to the line electrodes of the heaters, having moderate resistances of 65–70 Ω, resulting in local heating due to resistive losses. The RTDs utilize the known relationship between the resistivity of Ni and temperature to deduce temperature readings based on 4-point resistance measurements and were calibrated using measurements of resistance at different known temperatures (ESI† section 1). By using an array of heaters and sensors, it was possible to provide temperatures to the microfluidic device *via* two different spatial configurations, *i.e.* i) each heating zone can be set to a constant temperature, or ii) the heaters can create a linear temperature gradient across the microfluidic device.

Cooling of the heat-stage was achieved by flowing deionized water through a 120 μm deep and 12 mm wide channel embedded in the glass substrate of the heat-stage. The cooling channel was fabricated through wet etching and fusion bonding of two separate glass wafers. To find a suitable design of the cooling system, heat transfer was modelled using FEM in COMSOL to compare active and passive cooling. From this (data not shown), we concluded that active liquid cooling stretching several mm outside of the temperature control window provides the best performance. The resulting design is displayed in Fig. 1A and S5B.† Further, the cooling channel was deliberately placed between the objective and the Joule heaters to prevent heating of high-magnification objectives where immersion oil could act as a thermal bridge.

For cell experiments, the heat-stage was assembled with a PDMS–glass microfluidic chip. The microfluidic chip was

assembled on top of the heat-stage by adding a drop of immersion oil in between the two devices. The three single-cell arrays of the microfluidic chip (each with 5500 microwells across an area of 1.53 mm × 5.80 mm) were aligned to the heaters under a stereo microscope (Fig. 1B and S5†). Scotch tape was added to secure the attachment of the chip.

The temperature-controlling unit (Fig. 1D) interfaces the heat-stage with the software. The unit delivers power to the heaters, transduces the signals from the RTDs and controls the feedback system. Temperatures were set by modifying the power levels supplied to the heaters *via* pulse-width-modulation. Here, each heater was connected to a supply voltage of 12 V in series with an NPN switching transistor, which was in turn connected to ground. The transistor was switched ON and OFF by the pulse-with-modulated signal from the microcontroller with a 12 bit resolution in a given duty cycle and, hence, the applied power across the heaters could be controlled with the same resolution. The RTDs were transduced by the temperature controller using RTD-to-digital converters with a resolution of up to 0.0534 °C. A detailed description of the hardware of the system is found in ESI† section 4.

Temperature regulation. The stage can be run in two modes of operation: manual mode, where the user selects the powers applied across each heater, or automatic mode, where the user selects set-point temperatures. In automatic mode, the temperature controller unit regulates the applied powers to the heaters based on temperature read-outs from the sensors using six independent proportional–integrational (*PI*) controllers, one for each heater (Fig. 1D and ESI† section 3). Each controller has two inputs (set-point and measured temperature) and one output (power-level of the heater). The P and I coefficients are stored on the microcontroller and, to achieve adaptive functionality, it was possible to modulate all coefficients by a common factor, *e.g.* for slow ramping to avoid temperature overshoot when turning the system on. USB serial communication was established between the temperature controller and the computer *via* a GUI software program (Python 3.7). This enabled monitoring and logging of data and provided a means for the user to set different temperature set-points and profiles.

Even though the preferred mode of operation for any application is automatic mode as this allows the operator to select temperatures rather than power levels, the inherent properties of the heat-stage are best characterized by running it in manual mode. For this evaluation, the power applied to the heaters was increased from 0 to a constant value of 300 mW at $t = 0$. The responses of the six heaters were analyzed to find steady-state temperatures, time constants and sensitivities for different flow rates of cooling liquid (Fig. S1†). The experiments were repeated with and without a reference chip attached to the heat-stage to mimic the effect of having a microfluidic device attached to the heat-stage and to evaluate the resulting heat transfer. The time constants, τ, which are found by modelling the response as a first order system, demonstrated a decrease with increasing flow rate and an increase as the reference chip was placed on the stage (ESI† section 2). Under normal operating conditions (with the chip attached and 60 μl min^{-1} cooling flow), τ was in the order of 150 s and reached a steady-state temperature of about 50 °C when applying 300 mW. The sensitivity, which is calculated as the applied power divided by the steady-state temperature, was largely independent of whether a chip was present on the stage or not (ESI† section 2). A higher sensitivity, as seen for low cooling liquid flow rates, requires a high resolution of the applied power to be able to fine-tune the desired temperatures. The 12 bit resolution, *i.e.* 4092 discrete power levels, facilitated in the temperature regulation system met this demand. For the lower sensitivity, seen for high cooling liquid flow rates, a higher maximum power is required to be able to achieve a fast response when operated in automatic mode. In this study, the maximum power was limited to 300 mW; however the same hardware would be able to operate at powers up to 2.4 W, a limit which is set by the switching transistors with a maximum allowed current of 200 mA at 12 V.

The resulting sensitivities and time constants have implications on the optimization of the P and I coefficients of the temperature controller. As the sensitivity is essentially independent of loading the stage with a chip, the P coefficient could be set as the same value for different chips. However, the sensitivity and hence the P coefficient are dependent on the cooling flow rate. Time constants depend on both the chip and flow rate, and therefore, the I coefficient has to be optimized for each given flow rate and chip size in this study. In future work, this could be implemented by using adaptive tunings, which are functions of both the measured flow rate and the mass of the chip.

For operation in automatic mode, the P and I coefficients of the controller were selected as a trade-off between rapid temperature change and avoiding any temperature overshoot. It should be noted that as the feedback loop runs continuously, the temperature of the stage will remain at the desired setting despite drift in the steady-state temperature of the heaters or changes in the environment, such as room temperature or placement of a microfluidic chip on the stage. Thermally responsive liquid crystal sheets were used to confirm the uniformity of the temperatures across the temperature control stage and only minor deviations were detected (Fig. S3†). In this work, we demonstrated temporal temperature profiles with step-wise increasing and oscillating profiles as well as a spatial linear temperature gradient across the area (Fig. 2). In addition, the versatility of the temperature regulation system makes it possible to produce a wide set of other spatiotemporally controlled temperatures, which are not described here.

Short- and long-term temperature exposures of single *Symbiodinium* cells

Using the temperature regulation system, the thermal response of single cells of *Symbiodinium* to moderate thermal stress (22–

40 °C) was assessed. To quantify the photometabolic effect of temperature stress on single cells, variable chlorophyll fluorimetry (PAM) imaging was used to measure the PSII maximum quantum yield under dark conditions, F_v/F_m. For these experiments, two strains of *Symbiodinium*, *i.e. Symbiodinium microadriaticum* (CCMP2467, clade A1[24]) and *Effrenium voratum* (CCMP421, clade E[24]), were used. Cells from each strain were immobilized within a microfluidic array containing 16 500 microwells, which was subsequently attached to the heat-stage. During all thermal exposure experiments, cells were kept under complete darkness.

Thermal stress can affect the stability of photosystem constituents and repair processes,[3] which can affect the cells' ability to photosynthesize. Previous experiments[25] systematically tested the timing of thermal adaptation in *Symbiodinium* by growing cells at 25 °C, transferring them to 30 °C and subsequently measuring their F_v/F_m at different time intervals. This revealed that 6 h of incubation at 30 °C significantly enhanced the thermal tolerance of *Symbiodinium* (compared to 0 h of incubation) and that this thermal acclimation was associated with *de novo* synthesis of proteins. The time required for *de novo* synthesis of proteins (~6 h) was thus considered a suitable duration of thermal acclimation in our experiments with *Symbiodinium*.

To quantify the effect of varying durations of temperature stress on *Symbiodinium*, three different temperature experiments were performed:

i) *Short-term:* single cells were exposed to a step-wise increase of +1 °C each with a duration of 15 min per step,

ii) *Long-term:* single cells were exposed to a step-wise increase of +1 °C each with a duration of 6 h per step

iii) *Sinusoidal:* single cells were exposed to a sinusoidal temperature profile with a period of 30 min and repeated several times.

Our *a priori* assumption for experiments i) and ii) was that cells exposed to short-term thermal stress (<6 h) would not be able to acclimate their photometabolism to elevated temperatures, whereas cells exposed to long-term thermal stress (>6 h) would have enough time to do so. Based on previous works,[26–28] we also expected considerable heterogeneity among single cells of *Symbiodinium* in their ability to withstand thermal stress events.

Time-resolved temperature exposures were accomplished by running the temperature regulation system in automatic mode. During the start-up procedure, the adaptive functionality of the temperature controller was used where the *P* and *I* coefficients were reduced by a common factor to avoid any risk of temperature overshoot when setting a pre-conditioning state at 22 °C, which is the nominal cultivation temperature of *Symbiodinium*. After start-up, the *P* and *I* coefficients were set back to their optimized values, giving +1 °C step-increase in about 40 s with minimal overshoot (~0.1 °C for each step-increase). It is noted that the noise level of the read-out from the RTDs increased for higher temperature, an effect that is attributed to thermal noise generated by some of the electrical components (Fig. S2†).

Short-term thermal exposure. Thermal stress was applied using a step-wise increasing temperature profile. Temperature treatments started 75 min after the nominal cultivation temperature (=22 °C) of both strains was reached and involved a step-wise increase by +1 °C until a final temperature of 36 °C was reached. Each temperature increase lasted 15 min and throughout the experiment F_v/F_m was assessed every 5 min. Pre-stimulus F_v/F_m values were calculated by taking the average of the last five F_v/F_m measurements at 22 °C (immediately before elevated temperatures were applied). For each temperature treatment, average values of F_v/F_m were calculated by taking the mean of the three F_v/F_m measurements per treatment. For all measured cells F_v/F_m decreased as temperature increased (Fig. 3A and B for each strain, respectively) but stepwise increasing temperatures revealed a distinct difference in photophysiology between the two *Symbiodinium* strains. For example, a temperature exposure of +5 °C caused a 13% reduction in F_v/F_m in strain CCMP2467, compared to average pre-exposure values (=22 °C) while the same temperature exposure caused only a 5% decrease in CCMP421. These strain-specific differences in photophysiology persisted at further elevated temperatures, where *e.g.* a temperature exposure of +8 °C decreased F_v/F_m by 45% in CCMP2467 but only by 11% in CCMP421 and an exposure to +11 °C caused a reduction of F_v/F_m by 91% in CCMP2467 and but only 18% in CCMP421. Only CCMP421 maintained photosynthetic functioning above the noise floor of the chlorophyll fluorometer (<0.05) at a temperature of +12 °C. All other reductions of F_v/F_m at a given temperature (compared to pre-stimulus conditions) are summarized in ESI,† Table S1. No recovery of F_v/F_m was observed in either of the two strains after the end of the temperature stress treatments (data not shown). Together, these data demonstrate that *Symbiodinium* CCMP2467 is more sensitive towards short-term thermal stress than *Symbiodinium* CCMP421.

Long-term thermal exposure. To determine whether prolonged thermal stress leads to acclimation between *Symbiodinium* CCMP2467 and CCMP421, single-cells of each strain were exposed to step-wise increasing temperatures with a duration of 6 h per step. Temperature treatments commenced 6 h after the nominal cultivation temperature of both strains (=22 °C) was reached and involved the step-wise increase by +1 °C until a final temperature of 33 °C or 35 °C was reached for CCMP2467 or CCMP421, respectively (Fig. 3C and D). Here, F_v/F_m was assessed every 15 min (*cf.* every 5 min for the short-term exposures) as the long experimental duration gave a sufficient number of data points. The reduction of F_v/F_m upon exposure to different stepwise increases in temperatures is summarized in ESI,† Table S1. Similar to previous short-term temperature exposures, prolonged temperature stress caused notable differences in photophysiological responses in both strains of *Symbiodinium*. For example, a temperature exposure of +5 °C decreased F_v/F_m by 29% in CCMP2467 but only 6.7% in CCMP421. This trend continued at further elevated

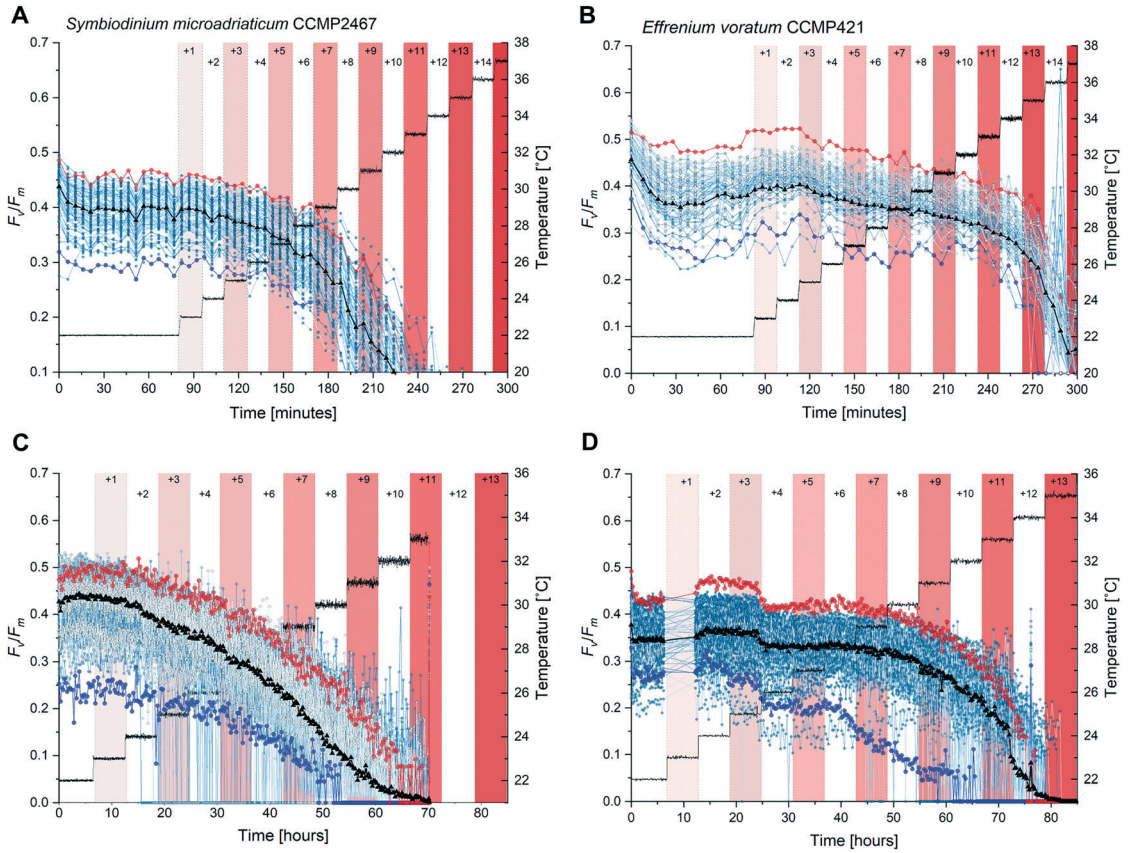

Fig. 3 Short-term and long-term temperature exposures cause photophysiological differences among single cells of *Symbiodinium* CCMP2467 and CCMP421. (A) and (B) Single-cell maximum quantum yields (F_v/F_m) under incrementally increasing temperatures of short durations (15 min) for *Symbiodinium* CCMP2467 (A) and CCMP421 (B). Single cells were exposed to stepwise temperature treatments of +1 °C. Each temperature treatment is indicated by alternating red and white color bars. During the entire experiment F_v/F_m was assessed every 5 min and cells were otherwise kept in the dark. Right *Y*-axis and corresponding thin gray line: average temperatures as measured by sensors on the heating stage. Note the photophysiological traces of single-cells performing better (red circles, 2SD above) or worse (blue circles, 2SD below) than the population average (black triangles). (C) and (D) Single-cell maximum quantum yields (F_v/F_m) under incrementally increasing temperatures of long durations (6 h) for *Symbiodinium* CCMP2467 (C) and CCMP421 (D). Single cells were exposed to stepwise temperature treatments of +1 °C, each for a duration of 6 h. During long-term thermal exposures F_v/F_m was assessed every 15 min and cells were otherwise kept in the dark.

temperatures, where *e.g.* a temperature exposure of +8 °C caused a reduction of F_v/F_m by 71% in CCMP2467 but only 12.5% in CCMP421. The photosynthetic activity of CCMP2467 was entirely inhibited ($F_v/F_m < 0.05$) at 32 °C (+10 °C) while this inhibition occurred at a temperature of 34 °C (+12 °C) for CCMP421. Together, this data demonstrate that *Symbiodinium* CCMP2467 is more sensitive towards long-term thermal stress than *Symbiodinium* CCMP421.

Long-term temperature exposures consistently caused more dramatic declines in F_v/F_m than short-term temperature exposures. For example, in CCMP2467 temperatures of +5 °C reduced F_v/F_m by 13% in short-term exposures and by 29% in long-term exposures. In CCMP421, a similar effect was observed, although less pronounced. Here, short-term exposures to +5 °C reduced F_v/F_m by 4.7%, whereas long-term exposures caused a reduction of 6.7%. These data suggest that prolonged thermal stress exposure decreases the ability of both *Symbiodinium* CCMP2467 and CCMP421 to effectively photosynthesize when compared to short-term thermal exposures. At first, these result seem to contradict our hypothesis on metabolic adaptation of the *Symbiodinium* strains but further analysis of the relationship between intensity and duration of thermal stress is given in section 2.5.

The observed variability in single-cell F_v/F_m between both strains of *Symbiodinium* was high, both during pre-stimulus conditions (*i.e.* 22 °C) and during elevated temperatures (Fig. 3). Measuring and tracking this variability over the entire experimental duration enabled the identification of single cells with F_v/F_m values that were two standard deviations (SD) above or below the population average as marked in red and blue, respectively (Fig. 3). Notably, cells with above average values of F_v/F_m consistently outperformed cells with below average values of F_v/F_m in their ability to withstand increasing thermal stress throughout experiments. These data highlight that populations of single cells contain variable phenotypes which differ in their ability to withstand temperature stress of varying durations. Such population characteristics go undiscovered in typical bulk approaches yet could be exploited to, *e.g.*, select specific cells with desirable traits for the assisted evolution of *Symbiodinium* or other biotechnologically important unicellular microalgae.

Exposure to repeated sinusoidal temperature profiles. In most environments, temperature varies over time due to day/night cycles and seasonal changes in the incident angle of solar irradiation. A unique feature of the herein presented temperature regulation system is that these changes in temperature environments can be reconstructed and presented to cells of interest. To study how thermal stress of oscillating temperatures affects single-cell F_v/F_m, *Symbiodinium* CCMP2467 cells were exposed to sinusoidal temperature cycles between 22 °C and 35 °C with a period of 30 min following a pre-stimulus at 22 °C for 1 h 20 min. Here, the experiment was designed to give the same total thermal dose as the short-term stepwise increasing temperature profile (see section 2.5 for discussion on thermal dose). The temperature profile and average F_v/F_m of the population are presented as a function of time in Fig. 4. Single-cell responses are provided in Fig. S7.† The average F_v/F_m oscillates with the same period as the temperature variations, but with an approximate delay of 5 min between the highest applied temperature (35 °C) and the corresponding local minima in the average F_v/F_m. After repeated exposure to sinusoidal temperatures, the average F_v/F_m declines progressively. Measurements of F_v/F_m demonstrate that cells start to recover at the end of the experiment (t = 9 h), after being given fifteen repeated sinusoidal temperature exposures. The dynamics of this recovery have not been explored further, but could provide important clues on the relationship between exposure duration, magnitude and ability of cells to withstand varying thermal stress profiles. Together, these results demonstrate the capability of the temperature regulation system to reconstruct artificial and natural temperature profiles and provide them to cells immobilized in a microfluidic system.

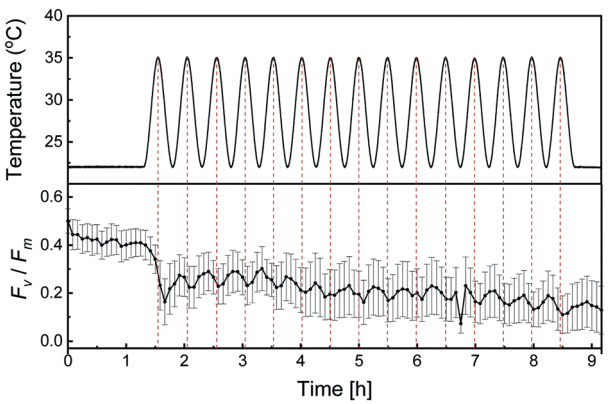

Fig. 4 Sinusoidal temperature profiles cause progressively declining F_v/F_m in *Symbiodinium* CCMP2467. The top part shows measured temperatures during the application of a sinusoidal temperature profile that oscillates from 22 °C to 35 °C with a period of 30 min. At t = 0 h, the heaters were turned on and set to regulate at 22 °C. At 1 h 20 min, the oscillating profile was started. At 7 h 20 min a constant temperature of 22 °C was set. The bottom part shows the population average of single-cell maximum quantum yields (F_v/F_m) when exposed to sinusoidal temperature cycles. Error bars indicate ±2 SD. During the entire experiment F_v/F_m was assessed every 5 min and cells were otherwise kept in the dark.

Spatial temperature gradients for parallelized assessment of photosynthetic responses

Beyond the dynamic control of temperatures, the temperature regulation system can also provide temperatures in the form of spatial gradients. Compared to discrete temperatures, gradients enable many different temperatures to be provided to arrays of immobilized cells simultaneously, which increases throughput but also comes at the cost of replication, that is, fewer cells per temperature are assessed when compared to discrete temperatures.

Temperature gradients were produced with good linearity for slopes ranging from 0.1 °C mm^{-1} to 2.5 °C mm^{-1}. The gradients used T = 24 °C as the set-point for the heater nearest the inlet of the cooling channel as shown in Fig. 5A. Regression analysis demonstrated linearity for 1.1 °C mm^{-1} (r^2 = 0.99992) (Fig. S2†). For slopes ranging from 0.5 °C mm^{-1} and below, r^2 decreased as the temperature differences approached the noise floor of the RTDs (Fig. S2†). At steep slopes, *i.e.* >1.5 °C mm^{-1}, the linearity was reduced as the cooling channel was unable to remove a sufficient amount of excess heat closest to the inlet. To expand the range of possible linear temperature gradients realized by future users, the flow rate of the cooling liquid could be increased (thereby increasing the cooling at the low temperature side) or the set-point temperature at the low temperature side could be increased (thereby increasing the temperature differences between the cooling liquid and the heat-stage surface). Either approach would result in improved linearity also at slopes above 1.5 °C mm^{-1}.

To qualitatively assess the photophysiological effects of a spatial thermal gradient, cells of *Symbiodinium* CCMP2467 were immobilized within microwells and assessed for their F_v/F_m. First, the cells were exposed to a homogeneous temperature of 25 °C (applied to all heaters for 20 min) and afterwards exposed to a linear temperature gradient ('stimulus') of 1.2 °C mm^{-1} for 6 h with a low temperature set-point of 25 °C. A temperature of 25 °C was chosen as a set point since previous experiments concluded that no severe effects on F_v/F_m were observed for temperatures lower than 25 °C (Fig. 3A and B). To visualize the temperature gradient, a thermally responsive liquid crystal sheet was placed on the stage (Fig. 5B and S3†) and the resulting color changes revealed a linear gradient across the active heating area. We attribute the small deviation from constant temperatures, along the lengths of the individual heaters and RTDs, to the laminar flow profile of the cooling liquid. Three zones were defined on the heat-stage along the thermal gradient ('inlet', 'middle' and 'outlet', referring to their position along the cooling channel) and the types of photophysiology of cells in these three temperature zones were compared (Fig. 5C and D). After 6 h of exposure to this thermal gradient, cells of *Symbiodinium* were assessed for their F_v/F_m, which revealed a 3.5% (inlet, n = 98), 12.7% (middle, n = 93) and 25.9% (outlet, n = 96) reduction in average F_v/F_m when compared to the average pre-stimulus F_v/F_m (n = 295, data from all heating arenas combined)

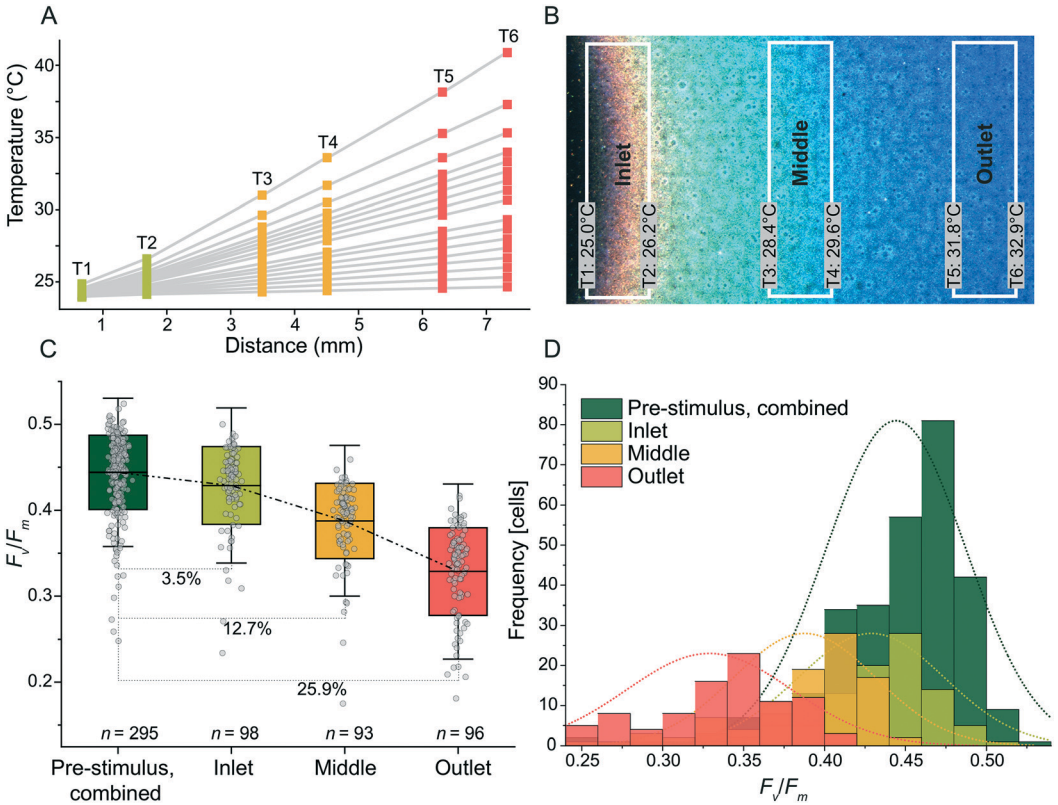

Fig. 5 Thermal gradients demonstrate a temperature-dependent decline in single-cell F_v/F_m of *Symbiodinium* CCMP2467. (A) Thermal linear gradients with slopes between 0.1 and 2.5 °C mm^{-1} were supplied along the horizontal axis of the heat-stage and accessed *via* the RTD array. The flow rate of the cooling liquid was 150 μl min^{-1} and the flow direction was from T1 to T6. A power limit of 400 mW for each heater was used. (B) The linearity of the thermal gradient was verified *via* a thermally responsive liquid crystal sheet (cross-over temperature: 30 °C), which was placed onto a coverslip *via* immersion oil and then mounted onto the heat-stage. The temperatures measured with the RTDs are indicated as well as the temperature zones defined for cell experiments ('inlet', 'middle', 'outlet'). (C) Exposure of *Symbiodinium* CCMP2467 to linear temperature gradients produced in (B) for 6 h. Note the reductions in F_v/F_m for the inlet, middle and outlet areas as compared to pre-stimulus assessment of F_v/F_m at 25 °C. (D) Histograms of F_v/F_m, before and after exposure to the linear temperature gradient. Note the progressive shift of normal distributions towards lower average values of F_v/F_m the closer the cells are to the outlet, the location with the highest temperature in the gradient.

(Fig. 5C). Histograms of F_v/F_m from before and after exposure to the temperature gradient (Fig. 5D) show a normal distribution that is progressively shifted towards lower average values of F_v/F_m the closer the cells are positioned to the outlet, *i.e.* the location of the highest temperature in the gradient. Together, this data supports that the heat-stage effectively delivers temperature gradients to immobilized cells of *Symbiodinium* and that it increased the throughput when operated in this mode. The reduction in F_v/F_m due to elevated temperature is, however, not directly comparable to the reduction that was achieved during short-term stepwise increases in temperature (Fig. 3A and B). We hypothesize that the stepwise increase in temperature causes different photophysiological responses than immediate exposure to single elevated temperature regimes.

Thermal dose analysis of *Symbiodinium* exposed to different thermal stress profiles

Previous experiments (short- and long-term stepwise increasing and sinusoidal temperature exposures) suggested that the photophysiology of *Symbiodinium* is not only affected by the magnitude of temperature elevation but also by the duration of the temperature elevation and by the shape of the temperature profile. To understand the relationship between temperature stimuli and photophysiology, we explored the use of a quantitative measure of the thermal dose.[29] To account for the time-dependence of the temperature in the different profiles, we here define the thermal dose as the cumulative temperature elevation from the start of the experiment to the investigated time-point, calculated *via* the following equation.

$$D = \int_{t_0}^{t_x} (T(t) - T_0)\mathrm{d}t \quad (1)$$

where D represents the thermal dose, t_0 the time at which elevated temperatures are first applied, t_x the investigated time-point, $T(t)$ the temperature as a function of time and T_0 the nominal cultivation temperature of cells (here 22 °C).

Single-cell data from short- and long-term temperature exposures (Fig. 3) and sinusoidal temperature exposures

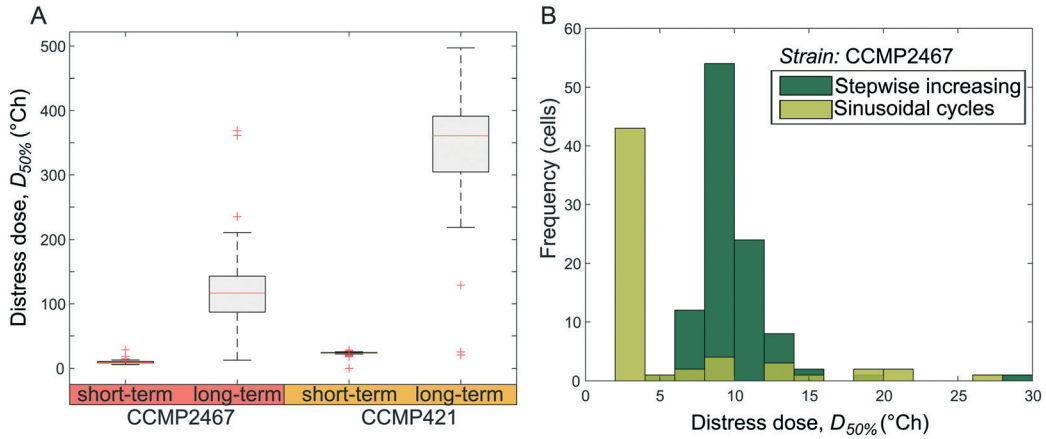

Fig. 6 Thermal dose analysis reveals the heat tolerance of cells exposed to different temperature profiles. (A) The distress dose, $D_{50\%}$ (the thermal dose at which cells' F_v/F_m values drop below 50% of their pre-stimulus F_v/F_m for the first time), is compared for short-term and long-term stepwise increasing temperature profiles for two *Symbiodinium* strains (CCMP421 and CCMP2467). The data show that long-term exposures of cells result in higher heat tolerance than short-term exposures. The central mark on each box is the median, the edges of the box are the 25th and 75th percentiles, the whiskers extend to the most extreme data points considered not to be outliers, and the outliers are plotted individually as red crosses. (B) Histogram distribution of distress doses, $D_{50\%}$, for cells exposed to short-term increasing and sinusoidal varying temperatures shows that the heat tolerance depends on the shape of the thermal exposure profile. Note that these two experiments were designed to give the same total dose for the same total time.

(Fig. 4) were analyzed to determine the thermal dose at which the photophysiology of *Symbiodinium* became substantially affected. In this study, cells were considered to be affected by temperature stress when their F_v/F_m decreased for the first time below 50% compared to pre-stimulus values (referred to as $D_{50\%}$ or distress dose). The resulting $D_{50\%}$ for stepwise increasing temperature profiles revealed that a majority of single cells from both *Symbiodinium* strains can withstand much higher accumulated thermal doses when these are applied for longer periods (here 6 h) rather than shorter periods (15 min) (Fig. 6A). This can be compared to the temperatures where F_v/F_m decreases below 50% of its initial value for the first time, which are lower for long-term exposures (CCMP2467 = 28 °C, CCMP421 = 33 °C) than short-term exposures (CCMP2467 = 31 °C, CCMP421 = 35 °C). A sustained feature of these measurements is that *Symbiodinium* strain CCMP421 is more resilient to temperature stimuli than CCMP2467, irrespective of whether the thermal stress is expressed in terms of temperature (Fig. 3) or thermal dose (Fig. 6A), or investigated in short-term (15 min) or long-term (6 h) experiments. To test whether the shape of a thermal exposure profile plays a role in determining the photophysiological effects in *Symbiodinium*, we designed sinusoidal temperature profiles to give the same thermal dose as those applied during short-term exposures. For both profiles, this enabled us to compare the relationship between accumulated thermal dose and specific temperatures for *Symbiodinium* CCMP2467 and revealed that cells on average withstood a higher thermal dose under short-term experiments than under sinusoidal experiments (Fig. 6B). We suggest that this observation is a result of the earlier exposure of cells to higher temperatures during sinusoidal experiments than during short-term experiments. Meanwhile, the spread in $D_{50\%}$ is larger for the sinusoidal profile than for stepwise increasing temperature exposures. Together these data support that the application of temperature profiles with an identical thermal dose results in different photophysiological outcomes between the two strains of *Symbiodinium*.

Conclusions

In this study we present a temperature regulation system that enables the generation of user-defined spatiotemporal temperature profiles. A unique feature of the temperature regulation system is its ability to rapidly and interchangeably connect with a range of microfluidic chips, thus increasing flexibility and reducing fabrication costs. A custom GUI software program executes spatiotemporal temperature profiles without prior programming expertise. In this study, we combined this temperature regulation system with microfluidics and single-cell chlorophyll fluorometry to measure the photophysiological response of two strains of *Symbiodinium* (CCMP 421 and CCMP2467) to specific temperature profiles. By exposing immobilized single cells of *Symbiodinium* to long- and short-term increases in temperatures, gradients of temperatures and sinusoidal temperature cycles, we demonstrated that photophysiological responses depended on the exposure duration, exposure magnitude and strain background. A quantitative measure of the thermal dose, defined as the integral of the temperature elevation over time, revealed that cells of both strains withstood higher total thermal doses under long-term experimental conditions than under short-term conditions. This indicates that acclimation to elevated temperatures does occur among cells over the time-scales provided in this study. Lastly, analysis of single-cell data revealed heterogeneous

photophysiological responses between both *Symbiodinium* populations. We suggest that the herein presented combination of precise temperature regulation, microfluidics and non-invasive photophysiological imaging can be used to uncover the phenotypic variability among unicellular microalgae and enable the identification of temperature-resilient phenotypes for biotechnology and ecosystem restoration efforts. As the temperature regulation system can easily be combined with alternative microfluidic devices, we foresee its application to other research avenues such as mammalian cell research and microbiology.

Experimental

Fabrication of the heat-stage

The cooling channel of the heat-stage was first formed using two 4″ glass wafers (0.2 mm and 0.7 mm, Borofloat 33, SCHOTT). A hard mask was deposited by sputtering (CS 730S, Von Ardenne) ~500 nm Mo on both sides of the 0.7 mm-thick wafer. The bottom side was protected and the top side was patterned by UV lithography (~12 μm AZ9260 spray resist, Microchemicals). Glass trenches were formed by wet etching in Mo etch (180 H_3PO_4 : 11 HAc : 11 HNO_3 : 150 H_2O) until the metal was etched through. This was followed by HF etching (49 wt%) to a depth of 120 μm. After stripping in acetone and Mo etch, the wafer was covered in a protective resist layer (S1813, Shipley, spin-cast at 6000 rpm). The fluid inlet and outlet were laser-cut using a pulse frequency of 10 kHz and a pulse peak power of 320 μW (AIO Go 4 mm, Östling marking systems, λ = 532 nm). The wafer was cleaned in acetone while sonicated in an ultrasonic bath.

Prior to bonding, the two glass wafers were cleaned using RCA-1 (1 : 1 : 5 NH_4OH : H_2O_2 : H_2O) and activated for bonding using HNO_3 (69 wt%) at 80 °C for 10 min, followed by rinsing in DI water. Directly after bonding by a light pressure, the wafer stack was thermally treated at 625 °C under ambient pressure for 6 h. A detailed protocol is provided in previous work.[30]

Next, thin-film electrodes were defined on the glass wafer stack. A flat top surface was achieved by recessing the electrodes into the glass. First, the solder pads were formed by UV lithography in an image-reversed resist layer (S1813, Shipley, spin cast at 6000 rpm) and trenches were wet etched in the glass using buffered HF (BOE 7 : 1, J.T. Baker). 2/400 nm Cr/Ni electrodes were defined by e-beam evaporation (PVD 75, Kurt J. Lesker Company) and lift-off in acetone. The electrode designs included the line electrodes of the Joule heaters and RTDs and were added using the same lithography process: UV patterning of an image-reversed resist layer (S1813, Shipley, spin cast at 6000 rpm), evaporation of 2/250/5 nm Cr/Ni/Au, and lift-off. Details are found in previous work.[23] The electrodes were annealed at 430 °C for 30 min in an Ar environment (Micro TF-6, Koyo Lindberg) and the wafer was diced (DAD 361, Disco) into individual chips. The resistances of the thin-film Joule heaters and RTDs, assessed with a handheld multimeter, were 65–70 Ω and 60–65 Ω, respectively.

Assembly of the temperature regulation system

The electric circuitry was distributed on two PCBs (Shenzhen JDB Technology Co.): one supporting the glass heat-stage with the integrated heaters and RTDs and one for the temperature control unit. The latter was based on a Teensy 3.6 microcontroller that delivered pulse width modulated control signals to NPN switching transistors (PMBT3904, Nexperia), which in turn supplied the heaters with ~12 V when switched ON. The microcontroller also detected the temperature of the sensors through a RTD-to-digital converter (MAX31865, maxim integrated) and preformed *PI* regulation using a C++ based software program. It was connected to a computer using a serial USB interface. A schematic of the circuit is found in ESI,† Fig. S4.

The electronic components were surface mounted onto the PCBs. Solder was dispensed using a 0.120 mm solder stencil and a screen printer (ProtoPrint S, LPKF). Components were placed using pick-and-place (ProtoPlace S, LPKF) and soldered using a soldering oven (Protoflow S, LPKF). Soldering was performed in two steps; first, the electrical components were soldered at 230 °C (SMD291AXT4, Chip Quik Inc), second, the thin-film Joule heaters and RTDs were soldered at 175 °C (SMDLTLFP10, Chip Quik Inc).

To connect the cooling flow, polyethylene tubing (ID 0.380 mm) containing an inner stainless steel tube support was mounted into the fluid interface. The tubing was then heated to 145 °C to form a seal and glue (Epo-tec 730, Epoxy Technology) was added to provide strain relief.

The heat-stage was finalized by attaching the PCB of the heat-stage to a 3D printed holder of microtiter plate format to provide a good fit in the microscope and to add the ability to align the microfluidic device (described below) with the heater array.

Cell culture

Non-axenic *Symbiodinium* strains CCMP421 (*Effrenium voratum*) and CCMP2467 (*Symbiodinium microadriaticum*) were purchased from the Bigelow culture collection. All *Symbiodinium* cultures were grown in f/2 medium prepared from autoclaved and sterile-filtered artificial saltwater (Instant Ocean, Aquarium systems, Sarrebourg, France) at a salinity of 36 ppt and a pH of 8.0 and without the addition of antibiotics. Cells were grown in Nunclon EasyFlasks with a volume of 25 cm^3 (ThermoScientific, MA) without shaking. All cultivars were maintained at 22 °C and white LEDs provided an irradiance (400–700 nm) of ~100 μmol photons m^{-2} s^{-1} over a 14 h/10 h day/night cycle. Two weeks prior to experiments, cells were inoculated in fresh f/2 medium at a 1 : 100 dilution, resulting in mid-exponentially growing cultures on the days of the experiments.

Cell experiments

Prior to cell experiments, the microfluidic device was filled with sterile f/2 medium. A culture of *Symbiodinium* cells (~6–8 ml) was mixed thoroughly, dispensed into Eppendorf vials

and centrifuged. The supernatant was removed and the cells were resuspended in ~50 μl f/2 medium. The cell suspension was injected into the microfluidic device until all microwells were visibly overlaid with cells. Loading of cells into the wells was achieved by manual compression of the flexible PDMS. The remaining cells were washed out by flushing with a pipette and fresh f/2 medium. A well size of 20 μm yielded a good compromise between loading efficiency, multiple cell occupancies and loss rate of cell populations for the investigated cell type as discussed previously.[26] Double and triple occupancies per-well were accepted in order to obtain higher loading efficiencies. Only wells containing single cells were used for the analysis, identified during post-processing using standard image analysis tools. The immobilization procedure caused no significant difference in F_v/F_m between unrestricted and immobilized populations of *Symbiodinium* (CCMP2467, p = 0.37; CCMP421, p = 0.75, two sample t-test, Fig. S6†). Following cell loading, the microfluidic chip was mounted onto the heat-stage by cleaning the stage with a lens wipe, adding a drop of immersion oil (Immersol 518N, Carl Zeiss, 20 μl) to the center of the stage and placing the microfluidic device, glass side down, in contact with the heat-stage. Bubble formation was rarely observed during this step and if it occurred the device was removed and the placement of the microfluidic device was repeated. Alignment of the array of microwells (with cells) with respect to the heaters was performed using a stereomicroscope. Both devices were positionally fixed using removable scotch tape.

The heat-stage with the microfluidic chip was combined with an upright multi-color variable chlorophyll fluorescence imaging microscope (IMAG-RGB; Heinz Walz GmbH, Germany). A detailed description of the microscope system can be found elsewhere.[31] Using the saturation-pulse-method, the maximum quantum yield of photosynthetic energy conversion in photosystem (PS) II, $F_v/F_m = (F_m - F_0)/F_m$, was measured in single cells of *Symbiodinium*. Here F_v, F_m and F_0 define the variable, maximal and minimal fluorescence of dark-adapted cells, respectively. Saturation pulses were provided by combining all three RGB (red-green-blue) light emitting diodes resulting in 'white light'. For both *Symbiodinium* species, visualization with a 10× objective (Zeiss Fluar 10×/0.5) yielded fluorescence readouts with ~500–1000 cells per field of view. No noticeable drift in XYZ was observed during experiments. Corrections of beam heterogeneities were made in ImagingWin based on acquired fluorescence images with a homogeneous fluorescence standard in conjunction with a built-in background normalization of subsequent experimental images. After experiments, light transmission images were combined with PAM image stacks within ImageJ[32] and registered to avoid artefacts arising from XY shifts. Single cells were manually identified within the light transmission image, and the resulting mask used to quantify F_v/F_m from chlorophyll fluorescence images using an in-house ImageJ script. During all experiments, cells within microwells were perfused with fresh f/2 medium, equilibrated to room temperature, using a non-pulsatile flow of 400 μl h^{-1} using low-friction 25 ml glass syringes (Hamilton 1000 series, Hamilton Corp.) mounted onto a syringe pump (neMESYS, Cetoni). The flow rate of cooling liquid in the heat-stage was set by applying 40 mbar to a pressure driven pump (MFCS-EZ, Fluigent), which resulted in a flow of about 60 μl min^{-1}.

Author contributions

MT and LB conceived, planned, supervised and provided funding for the study, contributed to parts of the experimental work and data analysis and prepared some of the visualization. MA and SJ contributed to the conceptualization of the work, planned, performed the experimental work and the data analysis. HB and LX performed experimental work and data analysis. SJ prepared the original manuscript draft onto which all the authors have contributed with writing, reviewing and editing. All the authors have read and approved the final version of the manuscript.

Conflicts of interest

There are no conflicts to declare.

Acknowledgements

The authors would like to thank Dr. Milena Moreira at Uppsala University for her support and contributions in initializing this project. This research has received funding from the European Research Council (ERC) under the European Union's Horizon 2020 research and innovation programme (grant agreement No 757444), the Knut and Alice Wallenberg Foundation (grant number WAF 2016.0112) and Uppsala University. L. B. was supported by grants from the Swedish Research Council (2019-04401) and the Science for Life Laboratory. Open access funding is provided by Uppsala University.

References

1 J. Ohlberger, *Funct. Ecol.*, 2013, **27**, 991–1001.
2 L. Muscatine, L. R. McCloskey and R. E. Marian, *Limnol. Oceanogr.*, 1981, **26**, 601–611.
3 S. Takahashi, S. M. Whitney and M. R. Badger, *Proc. Natl. Acad. Sci. U. S. A.*, 2009, **106**, 3237–3242.
4 E. M. Díaz-Almeyda, C. Prada, A. H. Ohdera, H. Moran, D. J. Civitello, R. Iglesias-Prieto, T. A. Carlo, T. C. Lajeunesse and M. Medina, *Proc. R. Soc. B*, 2017, **284**, 20171767.
5 P. Buerger, G. M. Schmidt, M. Wall, C. Held and C. Richter, *J. Exp. Mar. Biol. Ecol.*, 2015, **471**, 232–239.
6 P. Buerger, C. Alvarez-Roa, C. W. Coppin, S. L. Pearce, L. J. Chakravarti, J. G. Oakeshott, O. R. Edwards and M. J. H. van Oppen, *Sci. Adv.*, 2020, **6**, 1–9.
7 L. J. Chakravarti and M. J. H. van Oppen, *Front. Mar. Sci.*, 2018, **5**, 227.
8 M. Ackermann, *Nat. Rev. Microbiol.*, 2015, **13**, 497–508.
9 A. R. Wheeler, W. R. Throndset, R. J. Whelan, A. M. Leach, R. N. Zare, Y. H. Liao, K. Farrell, I. D. Manger and A. Daridon, *Anal. Chem.*, 2003, **75**, 3581–3586.

10 Ö. Baltekin, A. Boucharin, E. Tano, D. I. Andersson and J. Elf, *Proc. Natl. Acad. Sci. U. S. A.*, 2017, **114**, 9170–9175.
11 J. Ohan, B. Pelle, P. Nath, J. H. Huang, B. Hovde, M. Vuyisich, A. E. K. Dichosa and S. R. Starkenburg, *BioTechniques*, 2019, **66**, 218–224.
12 D. Di Carlo and L. P. Lee, *Anal. Chem.*, 2006, **78**, 7918–7925.
13 L. Armbrecht and P. S. Dittrich, *Anal. Chem.*, 2017, **89**, 2–21.
14 A. J. Mäki, J. Verho, J. Kreutzer, T. Ryynänen, D. Rajan, M. Pekkanen-Mattila, A. Ahola, J. Hyttinen, K. Aalto-Setälä, J. Lekkala and P. Kallio, *SLAS Technol.*, 2018, **23**, 566–579.
15 D. Nieto, P. McGlynn, M. de la Fuente, R. Lopez-Lopez and G. M. O'connor, *Colloids Surf., B*, 2017, **154**, 263–269.
16 S. Petronis, M. Stangegaard, C. B. V. Christensen and M. Dufva, *BioTechniques*, 2006, **40**, 368–376.
17 J. L. Lin, S. S. Wang, M. H. Wu and C. C. Oh-Yang, *Sensors*, 2011, **11**, 8395–8411.
18 H. Yan and H. Wu, *Encyclopedia of Microfluidics and Nanofluidics*, Springer Science+Business Media, New York, 2014, DOI: 10.1007/978-3-642-27758-0_758-2.
19 Z. Lei, D. Xie, M. K. Mbogba, Z. Chen, C. Tian, L. Xu and G. Zhao, *Lab Chip*, 2019, **19**, 1929–1940.
20 P. Neuzil, J. Pipper and T. M. Hsieh, *Mol. BioSyst.*, 2006, **2**, 292–298.
21 M. Safavieh, H. J. Pandya, M. Venkataraman, P. Thirumalaraju, M. K. Kanakasabapathy, A. Singh, D. Prabhakar, M. K. Chug and H. Shafiee, *ACS Appl. Mater. Interfaces*, 2017, **9**, 12832–12840.
22 A. J. De Mello, M. Habgood, N. L. Lancaster, T. Welton and R. C. R. Wootton, *Lab Chip*, 2004, **4**, 417–419.
23 M. Andersson, J. Ek, L. Hedman, F. Johansson, V. Sehlstedt, J. Stocklassa, P. Snögren, V. Pettersson, J. Larsson, O. Vizuete, K. Hjort and L. Klintberg, *J. Micromech. Microeng.*, 2017, **27**, 015018.
24 T. C. LaJeunesse, J. E. Parkinson, P. W. Gabrielson, H. J. Jeong, J. D. Reimer, C. R. Voolstra and S. R. Santos, *Curr. Biol.*, 2018, **28**, 2570–2580.e6.
25 S. Takahashi, M. Yoshioka-Nishimura, D. Nanba and M. R. Badger, *Plant Physiol.*, 2013, **161**, 477–485.
26 L. Behrendt, M. Mehdi Salek, E. L. Trampe, V. I. Fernandez, K. S. Lee, M. Kühl and R. Stocker, *Sci. Adv.*, 2020, **6**, 1–14.
27 D. A. Nielsen, K. Petrou and R. D. Gates, *ISME J.*, 2018, **12**, 1558–1567.
28 P. J. Ralph, A. W. D. Larkum and M. Kühl, *J. Exp. Mar. Biol. Ecol.*, 2005, **316**, 17–28.
29 H. O. Pörtner, *J. Exp. Biol.*, 2010, **213**, 881–893.
30 M. Andersson, K. Hjort and L. Klintberg, *J. Micromech. Microeng.*, 2016, **26**, 095009.
31 E. Trampe, J. Kolbowski, U. Schreiber and M. Kühl, *Mar. Biol.*, 2011, **158**, 1667–1675.
32 C. Schneider, W. Rasband and K. Eliceiri, *Nat. Methods*, 2012, **9**, 671–675.